

Symmetric exclusion processes on a ring with moving defects

Rakesh Chatterjee^{1,2 *} Sakuntala Chatterjee^{3 †} and Punyabrata Pradhan^{3‡}

¹ The Institute of Mathematical Sciences, CIT Campus, Taramani, Chennai 600113, India.

² Instituto de Ciencias Físicas, Universidad Nacional Autónoma de México, Cuernavaca 62210, México

³Department of Theoretical Sciences, S. N. Bose National Centre for Basic Sciences, Block-JD, Sector-III, Salt Lake, Kolkata 700098, India.

We study symmetric simple exclusion processes (SSEP) on a ring in the presence of uniformly moving multiple defects or disorders - a generalization of the model proposed earlier by us in Phys. Rev. E **89**, 022138 (2014). The defects move with uniform velocity and change the particle hopping rates *locally*. We explore the collective effects of the defects on the spatial structure and transport properties of the system. We also introduce an SSEP with ordered sequential (sitewise) update and elucidate the close connection with our model.

PACS numbers: 05.70.Ln, 05.40.-a, 05.60.-k, 83.50.Ha

I. INTRODUCTION

What happens when a system of interacting particles is subjected to a time-periodic forcing, which vanishes on average over a full cycle? Do the particles show directional motion and, if so, in which direction? These questions have recently attracted a lot of attention in the context of quantum or classical pumps [1–6], Brownian ratchets [7–9] and single-file motions of interacting colloids in the presence of ac driving forces [10–13], etc. On a more general ground, the effect of time-dependent potential on many-particle systems is of great interest in the context of externally stirred fluids, such as in microfluidic devices or in an assembly of nano- particles which could be driven by a periodically moving external potential [14–20]. In fact, recently, colloids in a moving optical trap have been of considerable theoretical interest [21–23] and have consequently been investigated in several experiments to understand static as well as dynamical aspects of fluctuations in nonequilibrium systems [24–27].

We consider the effect of periodically moving external potential, on a system of hard-core particles diffusing on a one dimensional lattice of length L , in a set-up of symmetric simple exclusion process (SSEP). Without any such potential, one has an SSEP with fixed (independent of space and time) hopping rates for the particles, which is an old problem [28] and has been intensively studied in the last few decades [29–39]. In the presence of a time-periodic potential, the hopping rates become explicit functions of time, which has not been explored much until recently [10, 11, 40]. Motivated by the recent experiments involving moving optical potential on colloidal particles [26], we model the external potential as ‘defects’ or disorders residing at particular sites where local diffusivity is different from the bulk of the system. These defects move around the periodic lattice with a

fixed velocity v , such that after a time interval L/v they complete one cycle, thus producing a time-periodic potential which drive the system away from equilibrium. In our earlier work [40], we had considered a single such defect which was shown to give rise to a travelling density wave, having a peak and a trough around the instantaneous defect-position and thus generating a particle current in the system. As the defect velocity v and the particle density ρ are varied, the particle current was shown to have rich behaviors, such as current reversal and multiple peaks [40].

In this paper, we consider multiple defects, all moving with the same velocity v , and investigate how their collective effects influence the transport properties of the system. For simplicity, we mainly focus on two defects and our results can be generalized to arbitrary number of defects. When the defects are placed far apart in the system, they act independently and their influence on the system can be described by using the results for the single-defect case [40]. However, when the defects are close to each other, the density patterns created individually around the single defects now start overlapping, which gives rise to interesting collective effects in the system. In particular, when the defects occupy next nearest neighbour sites on the lattice, a rather complex spatial pattern, with multiple peaks and troughs, emerges in the travelling density wave. Another remarkable effect is observed when the defects are closer further, i.e., when they are located in the nearest neighbor sites. In that case, the current in the system shows particle-hole symmetry for large defect velocity, although this symmetry was known to be violated in many of the earlier studies [10, 11, 13], including the single-defect case mentioned above [40]. Despite these qualitative differences, some of the interesting broad features obtained in our earlier work [40], such as polarity reversal and multiple peaks in particle current upon variation of v and ρ , still persist. We also discuss close connection between our model and an SSEP with sitewise ordered sequential update.

The organization of the paper is as follows. In the next section we define the model. In Sec. III we describe our results for multiple defects, with subsections A and B de-

*Electronic address: rakeshch@fis.unam.mx

†Electronic address: sakuntala.chatterjee@bose.res.in

‡Electronic address: punyabrata.pradhan@bose.res.in

voted to the cases when the defects are at nearest and next nearest neighbor positions, respectively. Subsection C contains results for the case when the defects are further apart. In Sec. IV we discuss SSEP with ordered sequential update and present our conclusions in Sec. V.

II. MODEL

The model is defined on a one dimensional periodic lattice of L sites where any site $i = 1, 2, \dots, L$ can be occupied by at most one particle. A particle can hop from an occupied site to one of the neighbouring empty site, with one of the following rates: (i) the hop rate from any of the defect sites to any the bulk sites is $p/2$, (ii) from one bulk site to a defect site is $r/2$ and (iii) all other hop rates are $q/2$ (see Fig. 1). Each defect resides at any particular site for a residence time $\tau = 1/v$ where v is the velocity of a defect. Without any loss of generality, we assume $v > 0$, i.e. at the end of the residence time the defect moves one site to the right.

When the defect velocity vanishes, $v = 0$, the hop rates satisfy detailed balance. Consequently, the ratio between the density $\rho_{i'}$ at a defect site i' and the density ρ_i at a bulk site i is given by $\rho_{i'}/\rho_i = \exp(-\beta V_0)$, with $\beta V_0 = \ln(p/r)$. Clearly, if $p > r$, the defect site has a lower density, ($\rho_{i'} < \rho_i$) and, if $p < r$, density at the defect site is higher than the bulk ($\rho_{i'} > \rho_i$); finite p and $r = 0$ (finite r and $p = 0$) corresponds to an infinite potential barrier (well).

For nonzero velocity v , the system is driven out of equilibrium and, after a long time, it reaches a time-periodic steady state where averages are periodic functions of time, with period L/v . In this state, a nontrivial density pattern, in the form of a travelling wave, emerges. For simplicity, in this paper, we mainly analyse the case with only two identical defects, both moving with the same velocity v , separated by a distance R . Note that $R = 0$ corresponds to the case when both the defects are present on the same site, i.e. only one defect site is present in the system. This case has already been studied in [40]. We will separately consider three situations, (a) $R = 1$ when the defects are present at adjacent sites, (b) $R = 2$, the defect sites are next nearest neighbors and (c) $R \geq 3$, when the defect sites are further apart. Our analysis can be easily extended to larger number of defects.

III. MULTIPLE MOVING DEFECTS

The configuration of the system is specified by the occupancy of each site and the position of the defect sites. Let $\{\eta_i^{\alpha_1, \alpha_2}\}$ denote the occupancy variable that takes the value 1 (0) if the i -th site is occupied (empty) when the two defects are located at sites α_1 and α_2 . Starting from an initial configuration, the system eventually reaches a time-periodic steady state where the averages, such as the

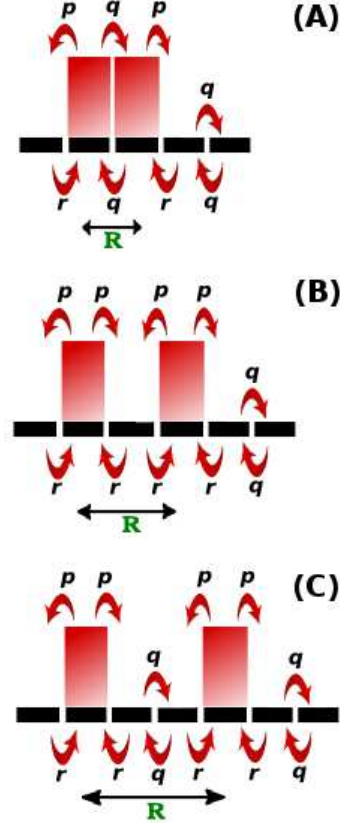


FIG. 1: (Color online) Schematic representation of the model. Two defects reside at two sites which are separated by a distance R as shown in (A) $R = 1$, (B) $R = 2$, (C) $R = 3$. Particle hopping is possible from a particular site if the site is occupied and the destination site is empty. The hopping rate from a defect site to a bulk site is p and the reverse process occurs with rate r (for barrier-type defect, $p > r$; for trap-type defects, $p < r$). All other hopping rates are q . A defect resides at a particular site for a residence time $\tau = 1/v$ and then moves to the nearest neighbour site, say, in the clockwise direction.

local density $\rho_i^{\alpha_1, \alpha_2}(t) = \langle \eta_i^{\alpha_1, \alpha_2}(t) \rangle$ at any site i , are periodic functions of time, with a period L/v . The residence time of the defect at a site is $\tau = 1/v$ and from now onwards, unless stated otherwise, we make all the measurements only at discrete times $t = m\tau$ ($m = 0, 1, \dots, \infty$), when the defects are about to leave a site and move onto the next one. The density pattern created around each defect site also moves with the defect with the same velocity v . Therefore, at any time t , the time evolution of the local density $\rho_i^{\alpha_1, \alpha_2}(t)$ can be written in a matrix form as given below,

$$\langle \rho^{\alpha_1+1, \alpha_2+1}(t + \tau) | = \langle \rho^{\alpha_1, \alpha_2}(t) | \mathcal{W}^{\alpha_1+1, \alpha_2+1}, \quad (1)$$

where i -th element of the row vector,

$$\langle \rho^{\alpha_1, \alpha_2}(t) | \equiv \{ \rho_1^{\alpha_1, \alpha_2}(t), \dots, \rho_i^{\alpha_1, \alpha_2}(t), \dots, \rho_L^{\alpha_1, \alpha_2}(t) \}, \quad (2)$$

denotes the local density at site i and the elements of the time-evolution operator $\mathcal{W}^{\alpha_1, \alpha_2}$ is the transition matrix provided that the defects reside at sites α_1 and α_2 . By definition, in the time-periodic steady state, density $\rho_{st,i}^{\alpha_1, \alpha_2}$ at site i has the following property

$$\rho_{st,i+1}^{\alpha_1+1, \alpha_2+1} = \rho_{st,i}^{\alpha_1, \alpha_2}, \quad (3)$$

which will be used later to the find the exact structure of the density profile. Similarly, the time evolution equations for n -point correlations $\langle \eta_i^{\alpha_1, \alpha_2}(t) \eta_{i+1}^{\alpha_1, \alpha_2}(t) \dots \eta_{i+n-1}^{\alpha_1, \alpha_2}(t) \rangle$ and their steady-state profile can be constructed. However, it is not easy to analytically solve the full Bogoliubov-Born-Green-Kirkwood-Yvon (BBGKY) hierarchy of the coupled equations involving n -point spatial correlations. Therefore, in this paper, we confine ourselves to only the mean-field analysis of Eq. 1, which in fact captures the broad features of the model quite well.

Our immediate task now is to obtain the elements of the transition matrix $\mathcal{W}^{\alpha_1, \alpha_2}$. As we shall see in the following sections, the transition matrix elements actually depend on two-point correlations and, within mean-field approximation, determines the structure of the travelling density wave and the particle current in a self-consistent way. For the most part of the paper, we focus on the case of infinitely large potential barrier ($r = 0$).

A. $R = 1$: two nearest neighbor defect sites with infinite potential barrier

Let us denote the defect positions at one particular configuration as $\alpha_1 = \alpha$ and $\alpha_2 = \alpha+1$. We first consider the case when there is no bulk hopping in the system, i.e. $q = 0$. Since infinite potential barrier corresponds to $r = 0, p \neq 0$, a particle can only hop out of a defect site into the bulk. Two defect sites being in the adjacent positions, this means a particle can hop only from site α to site $\alpha - 1$ and from site $\alpha + 1$ to site $\alpha + 2$. In other words, only the following two transitions (each occurring with rate p) are possible in the system: (a) $0\hat{1}\hat{X} \rightarrow 1\hat{0}\hat{X}$ and (b) $\hat{X}\hat{1}0 \rightarrow \hat{X}\hat{0}1$. Here we have denoted the defect sites by cap and X can be either 0 or 1. The transition matrix element $\mathcal{W}_{i,j}^{\alpha+1, \alpha+2}$, the probability that a particle at site i hops to site j within the defect residence time τ , can be written as,

$$\begin{aligned} \mathcal{W}_{i,j}^{\alpha+1, \alpha+2} &= 1 - a_- \quad i = j = \alpha + 1 \\ \mathcal{W}_{i,j}^{\alpha+1, \alpha+2} &= 1 - a_+ \quad i = j = \alpha + 2 \\ \mathcal{W}_{i,j}^{\alpha+1, \alpha+2} &= a_+ \quad i = j - 1 = \alpha + 2 \\ \mathcal{W}_{i,j}^{\alpha+1, \alpha+2} &= a_- \quad i = j + 1 = \alpha + 1 \end{aligned} \quad (4)$$

where all other off-diagonal elements are 0 and diagonal elements are 1.

Here, a_+ (a_-) is the conditional probability that a defect site, provided it is occupied, exchanges particle with its right (left) neighbour during the time-interval τ . For $R = 1$, the expressions for a_{\pm} is particularly simple and is given by

$$\begin{aligned} a_+ &= \left[\frac{\langle \eta_{\alpha+1}^{\alpha, \alpha+1} (1 - \eta_{\alpha+2}^{\alpha, \alpha+1}) \rangle}{\kappa \langle \eta_{\alpha+1}^{\alpha, \alpha+1} \rangle} \right], \\ a_- &= \left[\frac{\langle (1 - \eta_{\alpha-1}^{\alpha, \alpha+1}) \eta_{\alpha}^{\alpha, \alpha+1} \rangle}{\kappa \langle \eta_{\alpha}^{\alpha, \alpha+1} \rangle} \right], \end{aligned} \quad (5)$$

where $1/\kappa(v) = (1 - e^{-p/2v})$ is the rate with which a local configuration $0\hat{1}\hat{X}$ or $\hat{X}\hat{1}0$ goes to $1\hat{0}\hat{X}$ or $\hat{X}\hat{0}1$, respectively, during time τ , assuming that the decay process is Poissonian.

To study the density profile, we consider a particular case when defects were at sites 1 and 2, and have just moved to the next sites. Then the corresponding transition matrix can be written in terms of a_+ and a_- as

$$\mathcal{W}^{2,3} = \begin{bmatrix} 1 & 0 & 0 & 0 & \dots & 0 \\ a_- & (1 - a_-) & 0 & 0 & \dots & 0 \\ 0 & 0 & (1 - a_+) & a_+ & \dots & 0 \\ \dots & \dots & \dots & \dots & \dots & \dots \\ 0 & 0 & 0 & 0 & 1 & 0 \\ 0 & 0 & 0 & 0 & 0 & 1 \end{bmatrix}.$$

Now we use with the following ansatz of the density profile, represented by the row vector

$$\langle \rho_{st}^{1,2} | = \{ \rho_-, \rho_b, \rho_+, \rho_b, \dots, \rho_b \}, \quad (6)$$

which must satisfy (as a property of the time-periodic steady state)

$$\langle \rho_{st}^{2,3} | = \langle \rho_{st}^{1,2} | \mathcal{W}^{2,3}, \quad (7)$$

where the row vector $\langle \rho_{st}^{2,3} |$ can be obtained by spatially translating (by one lattice unit) the density profile $\langle \rho_{st}^{1,2} |$:

$$\langle \rho_{st}^{2,3} | = \{ \rho_b, \rho_-, \rho_b, \rho_+, \rho_b, \dots, \rho_b \}. \quad (8)$$

Using the particle conservation

$$\rho_+ + \rho_- + (L - 2)\rho_b = L\rho \quad (9)$$

and Eq. 6, we solve for the ρ_{\pm} in terms of a_{\pm}

$$\rho_+ = \frac{\rho}{1 - a_+}, \quad \rho_- = (1 - a_-)\rho. \quad (10)$$

The above equations give an exact profile of the travelling density wave, which has a bump just in front of the rightmost defect site and has a trough separated from the bump by two lattice spacings, i.e., a trough at the leftmost defect site, as shown in Fig. 2. Note that, in the case of a single defect studied previously in [40], the bump was immediately followed by a trough, i.e., the gap between the bump and the trough was only one lattice

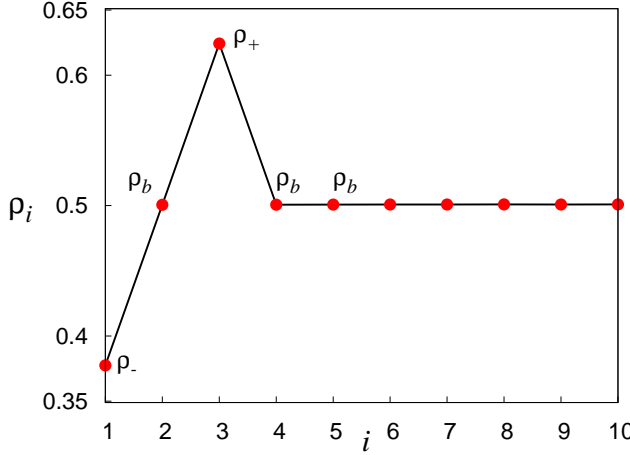


FIG. 2: (Color online) Time-averaged density profile of the travelling wave where the two defects are located at two adjacent sites, with defect velocity $v = 1.0$ for system size $L = 512$ and hopping rates $p = 1$ and $q = r = 0$. In this figure, the defects reside at sites 1 and 2, the bump is at site 3 and the trough is at site 1. Densities at all other sites are $\rho_b \approx \rho$, which equals to the global density in the limit of large system size $L \gg 1$.

spacing, as opposed to two lattice spacings here. As we show below, this qualitative difference gives rise to new interesting features like appearance of particle-hole symmetry in the current, albeit only in the regime of large defect-velocity.

Till now, the analysis remains exact. However, a_{\pm} still contains two-point density correlations (see Eq. 5) and needs to be calculated as a function of the global density ρ . As mentioned before, solving the hierarchy of equations involving many-point correlations is difficult and, therefore, we resort to a mean-field method, where we approximate two-point density correlations simply as a product of one-point correlations by writing $\langle \eta_{\alpha+2}^{\alpha, \alpha+1} \rangle \approx \rho_+$, $\langle \eta_{\alpha+2}^{\alpha, \alpha+1} \eta_{\alpha+3}^{\alpha, \alpha+1} \rangle \approx \rho_+ \rho_b$, $\langle \eta_{\alpha+1}^{\alpha, \alpha+1} \rangle \approx \rho_b$ and $\langle \eta_{\alpha}^{\alpha, \alpha+1} \eta_{\alpha+1}^{\alpha, \alpha+1} \rangle \approx \rho_- \rho_b$, to obtain the conditional probabilities

$$a_+ = \frac{(1 - \rho_b)}{\kappa} ; a_- = \frac{(1 - \rho_-)}{\kappa}. \quad (11)$$

Now we use Eqs. 10 and 11 to eliminate a_{\pm} and then Eq. 9 to obtain ρ_{\pm} as a function of global density ρ in the limit of large $L \gg 1$,

$$\rho_+ = \frac{\rho \kappa}{\rho + \kappa - 1} ; \rho_- = \frac{\rho(1 - \kappa)}{\rho - \kappa}. \quad (12)$$

Here, we have a rather simple closed form expression for ρ_{\pm} , unlike the case of a single defect in [40].

In Fig. 3, we plot ρ_{\pm} as a function of the global density ρ and the defect velocity v , for $p = 1$, $r = 0$ and $q = 0$ (red squares). The simulation results show good

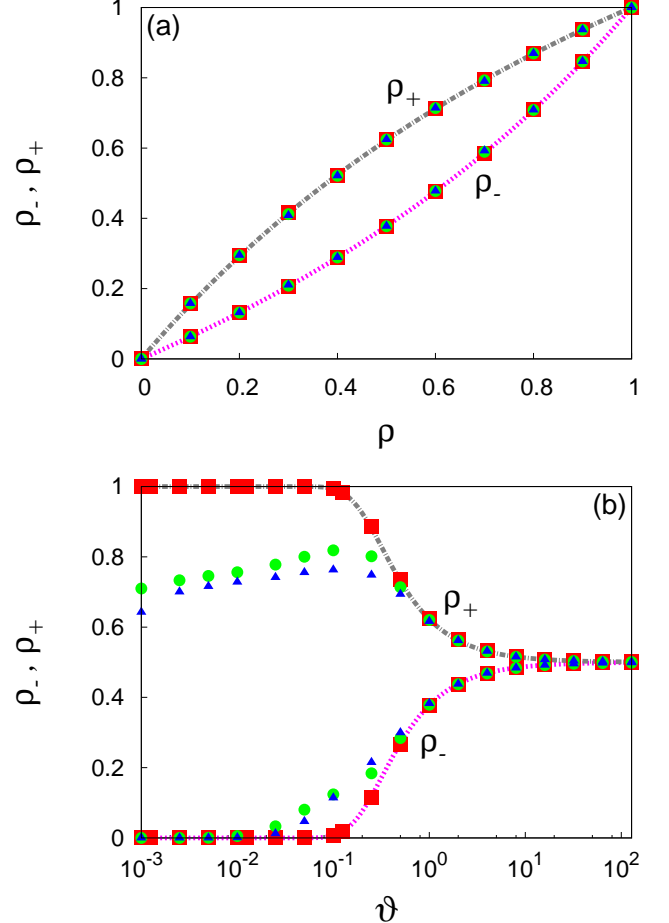


FIG. 3: (Color online) Two defects separated by distance $R = 1$. (a) ρ_+ and ρ_- are plotted against global density ρ where defect velocity $v = 1$ and $q = 0$ (red squares), 0.2 (green circles), 0.5 (blue triangles). (b) ρ_+ and ρ_- are plotted against defect velocity v where $\rho = 0.5$ and $q = 0$ (red squares), 0.2 (green circles), 0.5 (blue triangles). In all the cases, $L = 512$, $p = 1$, $r = 0$. Points and lines are simulation and mean-field theoretical results, respectively.

agreement with our analytical expression in Eq. 12. We also present our numerical results for $q \neq 0$ in the same plot. We find that for $v \gg q$, ρ_{\pm} do not depend strongly on q and Eq. 12 remains valid even for $q \neq 0$. However, for $v \lesssim q$ when the defect movement and bulk relaxation happen over similar time-scales, nontrivial correlations develop in the system and the above mean-field predictions break down, at least quantitatively; in Fig. 3b, one can see that, in the regime $v \lesssim q$, the deviations of the simulation results from the mean-field theory start creeping in. For very small defect velocity $v \ll p, q$, the system approaches an equilibrium state where the bump, expectedly, disappears (i.e., $\rho_+ \rightarrow \rho$) and the trough becomes completely devoid of any particle (i.e., $\rho_- \rightarrow 0$).

Using the fact that Eq. 12 remains valid for all q in the large v regime, one can calculate the current within

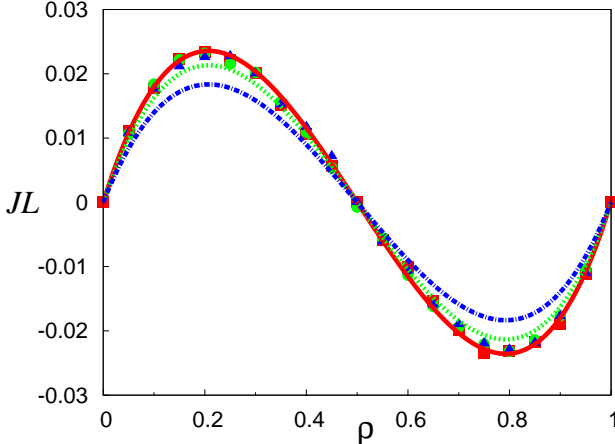


FIG. 4: (Color online) Two defects separated by distance $R = 1$. Scaled current JL is plotted against the global density ρ with defect velocity $v = 1.0$ and $L = 512$, $p = 1$, $r = 0$ for various values of $q = 0$ (red squares), 0.2 (green circles), 0.5 (blue triangles). The current is particle-hole symmetric and consequently vanishes at the half-filling $\rho = 0.5$.

mean-field theory for $v \gg q$. It is easy to see that during the time-interval τ , when the defect sites are at α and $\alpha + 1$, non-zero diffusive current exists only across four bonds in the system. Let $J_{i,i+1}$ denote the current across the bond between the sites i and $i + 1$. Then the non-zero contributions to current can be written as $J_{\alpha-1,\alpha} = \tilde{q}[\rho(1 - \rho_-) - \rho_-(1 - \rho)]$, $J_{\alpha,\alpha+1} = -\tilde{p}\rho(1 - \rho_-)$, $J_{\alpha+1,\alpha+2} = \tilde{q}[\rho(1 - \rho_+) - \rho_+(1 - \rho)]$ and $J_{\alpha+2,\alpha+3} = \tilde{p}\rho_+(1 - \rho)$, where the effective Poisson hopping rates are $\tilde{p} = (v/L)(1 - e^{-p/2v})$ and $\tilde{q} = (v/L)(1 - e^{-q/2v})$. By adding all of the individual contribution to the current, we obtain the net diffusive current averaged over a full cycle L/v ,

$$J_q(\rho, v) \simeq \tilde{q}[2\rho - \rho_- - \rho_+] + \tilde{p}[\rho_+(1 - \rho) - \rho(1 - \rho_-)]. \quad (13)$$

The above mean-field expression of current differs not only quantitatively from that in the single defect case (see Eq. 20 of Ref. [40]), but also qualitatively, because of the particle-hole symmetry in the current where $J_q(\rho, v) = -J_q(1 - \rho, v)$. It can be easily checked from Eq. 12 that under the particle hole transformation $\rho \rightarrow (1 - \rho)$, the height and depth of the bump and the trough, respectively, transform as follows: $\rho_+ \rightarrow 1 - \rho_-$ and $\rho_- \rightarrow 1 - \rho_+$. However, this holds only for large v , since the mean-field expression of current in Eq. 13 breaks down for $0 < v \ll q$, where correlations play a nontrivial role.

In Fig. 4, we plot scaled current JL (scaled by system size L) as a function of the global density ρ for various values of q , where defects move with velocity $v = 1.0$. The current is particle-hole symmetric and consequently vanishes for $\rho = 0.5$. For $q = 0$, the agreement between simulations and the mean-field theory as in Eq. 13 is excellent. However, some discrepancies between theory and

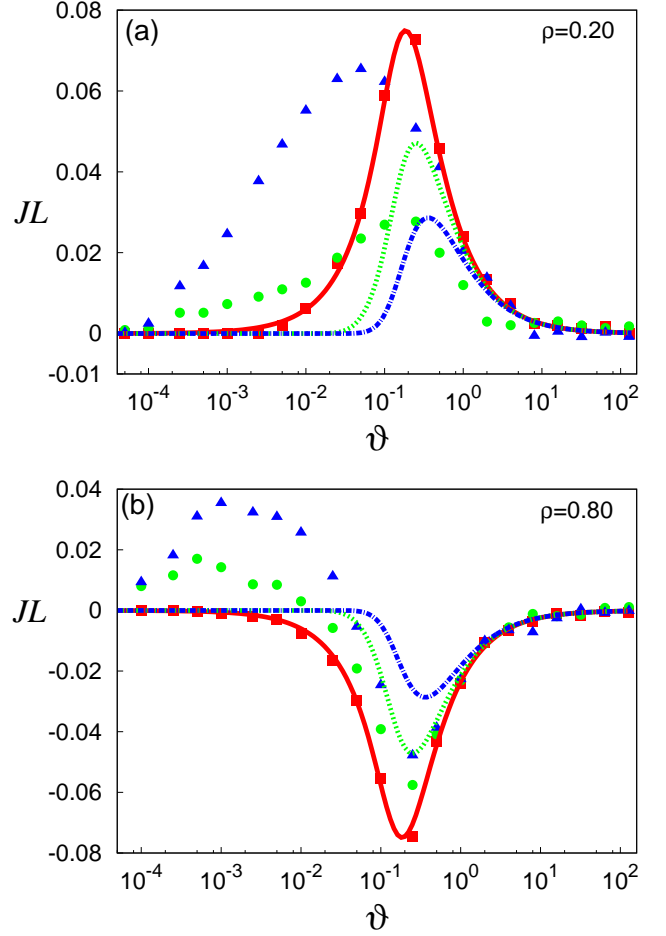


FIG. 5: (Color online) Two defects separated by distance $R = 1$. Scaled current JL is plotted against defect velocity v for two different values of densities (a) $\rho_1 = 0.2$ and (b) $\rho_2 = 1 - \rho_1 = 0.8$. Although mean-field theory predicts a particle-hole symmetry, for $0 < v \lesssim q$, this breaks down. Here $q = 0$ (red squares), 0.2 (green circles), 0.5 (blue triangles) with $L = 512$, $p = 1$, $r = 0$. The discrete points show simulation data and the continuous lines show mean-field predictions.

simulations are observed at larger values of q ; though the particle-hole symmetry is still found to be obeyed. In Fig. 5, we have plotted the scaled current JL as a function of defect velocity v for two different densities $\rho_1 = 0.2$ and $\rho_2 = 1 - \rho_1 = 0.8$, which are related to each other by the particle-hole transformation. At large velocities $v \gg q$, the mean-field theory captures quite well the broad features of the particle current. However, at the intermediate regime of velocity $0 \ll v \ll q$, the mean-field theory breaks down where the current, for nonzero q , is actually found to remain positive for both the densities $\rho_1 = 0.2$ and $\rho_2 = 0.8$, implying that the particle-hole symmetry is no more present at small values of v . Fig. 6 highlights this point, where we have plotted the scaled current as a function of density for a small value of $v = 10^{-3}$.

Above analysis can be easily generalised for arbitrary

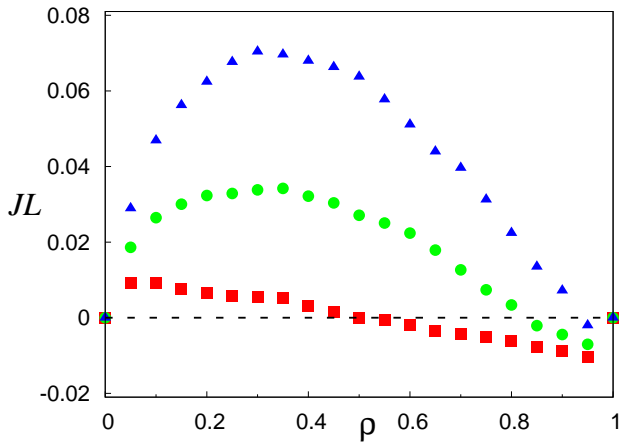


FIG. 6: (Color online) Two defects separated by distance $R = 1$. Numerical simulation results of scaled current JL is plotted as a function of the global density ρ for $q = 0$ (red squares), 0.2 (green circles), 0.5 (blue triangles) where the defect velocity $v = 10^{-3}$, $L = 512$ and $p = 1$ and $r = 0$. For intermediate and small values of defect velocity $0 < v \lesssim q \neq 0$, the absence of particle-hole symmetry in the current is quite evident.

number of defects located at consecutive n number of sites $\alpha_{k+1} = \alpha_k + 1$ with $k = 1, \dots, (n-1)$. The ansatz for the density profile needs to be suitably modified but many of the qualitative conclusions including existence of particle-hole symmetry remain valid.

B. $R = 2$: two next-nearest-neighbor defects with infinite potential barrier

In this section, we analyse the case where the defects are separated by two lattice spacings, i.e., if one defect is located at site α , the other one is located at site $\alpha + 2$. We first consider the case with $q = 0$. Our numerical simulation results for the density profile are shown in Fig. 7 where two bumps and two troughs can be seen. Motivated by this, we use the following ansatz for the density profile, measured at a time when the two defects are at sites 1 and 3,

$$\langle \rho_{st}^{1,3} | = \left\{ \rho_-^{(1)}, \rho_+^{(1)}, \rho_-^{(2)}, \rho_+^{(2)}, \rho_b, \dots, \rho_b \right\} \quad (14)$$

where there are two bumps and two troughs, placed alternately on four adjacent sites: first a trough of density $\rho_-^{(1)}$ and, then on the three right neighbours, a bump with density $\rho_+^{(1)}$, a trough with density $\rho_-^{(2)}$ and a bump with density $\rho_+^{(2)}$.

To study the density profile, we need to calculate the conditional probability $a_+^{(1)}$ (or $a_-^{(1)}$) that, during the time-interval τ , the occupied defect site α exchanges particle with its right (left) neighbour and the conditional

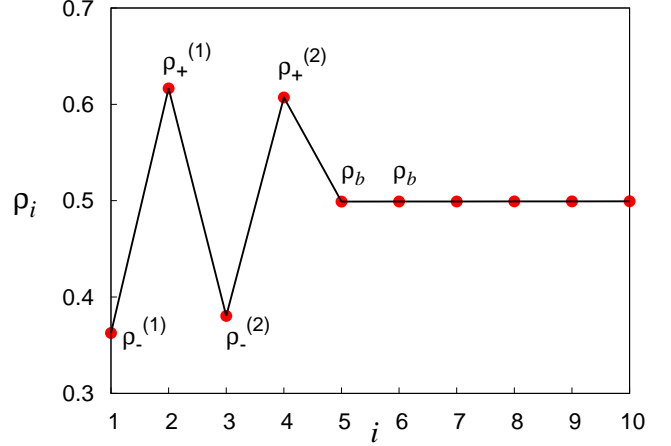


FIG. 7: (Color online) Two defects separated by distance $R = 2$. (here the defects reside at sites 1 and 3). Density profile for defect sites 1 and 3 shows two peaks $\rho_+^{(1)}, \rho_+^{(2)}$ and two troughs $\rho_-^{(1)}, \rho_-^{(2)}$. Bulk density is denoted by ρ_b .

probability $a_+^{(2)}$ ($a_-^{(2)}$) that, during the time-interval τ , the occupied defect site $\alpha + 2$ exchanges particle with its right (left) neighbour. For the case of $q = r = 0$, the non-vanishing transition rates occur only for the particles which are hopping from the defect sites, α and $\alpha + 2$, for which the transition matrix can be constructed in terms of these conditional probabilities as given below,

$$\mathcal{W}^{2,4} = \begin{bmatrix} 1 & 0 & 0 & 0 & 0 & 0 & \dots & 0 \\ a_-^{(1)} & \left(1 - a_+^{(1)} - a_-^{(1)}\right) & a_+^{(1)} & 0 & 0 & 0 & \dots & 0 \\ 0 & 0 & 1 & 0 & 0 & 0 & \dots & 0 \\ 0 & 0 & a_-^{(2)} & \left(1 - a_+^{(2)} - a_-^{(2)}\right) & a_+^{(2)} & 0 & \dots & 0 \\ 0 & 0 & 0 & 0 & 1 & 0 & \dots & 0 \\ \dots & \dots \\ 0 & 0 & 0 & 0 & 0 & 0 & \dots & 1 \end{bmatrix}$$

In the time-periodic steady state, the following condition must be satisfied

$$\langle \rho_{st}^{2,4} \rangle = \langle \rho_{st}^{1,3} \rangle \mathcal{W}^{2,4} \quad (15)$$

where the $\langle \rho_{st}^{2,4} \rangle$ is given by

$$\langle \rho_{st}^{2,4} \rangle = \left\{ \rho_b, \rho_-^{(1)}, \rho_+^{(1)}, \rho_-^{(2)}, \rho_+^{(2)}, \rho_b, \dots, \rho_b \right\}. \quad (16)$$

The steady-state condition Eq. 15 leads to the following set of four equations,

$$\rho = \rho_-^{(1)} + \rho_+^{(1)} a_-^{(1)}, \quad (17)$$

$$\rho_-^{(1)} = \rho_+^{(1)} \left(1 - a_-^{(1)} - a_+^{(1)} \right), \quad (18)$$

$$\rho_-^{(2)} = \rho_+^{(2)} \left(1 - a_-^{(2)} - a_+^{(2)} \right), \quad (19)$$

$$\rho_+^{(2)} = \rho_+^{(2)} a_+^{(2)} + \rho, \quad (20)$$

along with the particle number conservation,

$$\rho_-^{(1)} + \rho_+^{(1)} + \rho_-^{(2)} + \rho_+^{(2)} + (L-4)\rho_b = L\rho, \quad (21)$$

which can be solved to exactly obtain $\rho_\pm^{(1)}$ and $\rho_\pm^{(2)}$ in terms of the conditional probabilities $a_\pm^{(1)}$ and $a_\pm^{(2)}$,

$$\rho_+^{(1)} = \frac{\rho}{1 - a_+^{(1)}}, \quad (22)$$

$$\rho_-^{(1)} = \frac{\rho \left(1 - a_+^{(1)} - a_-^{(1)} \right)}{1 - a_+^{(1)}}, \quad (23)$$

The conditional probabilities $a_\pm^{(1)}$ and $a_\pm^{(2)}$ can be written in terms of three-point and four-point correlations as follows. First, we note that a particle can hop only from one of the two defect sites α and $\alpha+2$, either to the right or to the left, provided that the destination site is empty. To calculate $a_+^{(1)}$, we need to consider rightward hopping of a particle from the defect site α . For this hopping to take place, the site α must be occupied and the site $\alpha+1$ must be empty. In addition, it is crucial that within the residence time τ , no leftward hopping takes place from the other occupied defect site at $\alpha+2$ (as that would block the site $\alpha+1$) and no leftward hopping takes place from the defect site α (as the site α then gets empty). Therefore, in the calculation of $a_+^{(1)}$, the corresponding local configurations $1\hat{1}0\hat{0}$, $0\hat{1}0\hat{0}$, $1\hat{1}0\hat{1}$ and $0\hat{1}0\hat{1}$ (“cap” denotes the defect site, as before) are associated with different Poissonian decay rates $1/\kappa_1 = (1 - e^{-p/2v})$ and $1/2\kappa_2 = (1 - e^{-p/v})/2$ [40]

$$a_+^{(1)} = \left[\frac{\langle \eta_\alpha^{\alpha,\alpha+2} \eta_{\alpha+1}^{\alpha,\alpha+2} (1 - \eta_{\alpha+2}^{\alpha,\alpha+2}) (1 - \eta_{\alpha+3}^{\alpha,\alpha+2}) \rangle}{\kappa_1 \langle \eta_{\alpha+1}^{\alpha,\alpha+2} \rangle} \right] + \left[\frac{\langle (1 - \eta_\alpha^{\alpha,\alpha+2}) \eta_{\alpha+1}^{\alpha,\alpha+2} (1 - \eta_{\alpha+2}^{\alpha,\alpha+2}) (1 - \eta_{\alpha+3}^{\alpha,\alpha+2}) \rangle}{2\kappa_2 \langle \eta_{\alpha+1}^{\alpha,\alpha+2} \rangle} \right] + \left[\frac{\langle \eta_\alpha^{\alpha,\alpha+2} \eta_{\alpha+1}^{\alpha,\alpha+2} (1 - \eta_{\alpha+2}^{\alpha,\alpha+2}) \eta_{\alpha+3}^{\alpha,\alpha+2} \rangle}{2\kappa_2 \langle \eta_{\alpha+1}^{\alpha,\alpha+2} \rangle} \right] + \left[\frac{\langle (1 - \eta_\alpha^{\alpha,\alpha+2}) \eta_{\alpha+1}^{\alpha,\alpha+2} (1 - \eta_{\alpha+2}^{\alpha,\alpha+2}) \eta_{\alpha+3}^{\alpha,\alpha+2} \rangle}{2\kappa_2 \langle \eta_{\alpha+1}^{\alpha,\alpha+2} \rangle} \right] \quad (26)$$

Similarly, we obtain the other conditional probabilities

$$a_-^{(1)} = \left[\frac{\langle (1 - \eta_\alpha^{\alpha,\alpha+2}) \eta_{\alpha+1}^{\alpha,\alpha+2} \eta_{\alpha+2}^{\alpha,\alpha+2} \rangle}{\kappa_1 \langle \eta_{\alpha+1}^{\alpha,\alpha+2} \rangle} \right] + \left[\frac{\langle (1 - \eta_\alpha^{\alpha,\alpha+2}) \eta_{\alpha+1}^{\alpha,\alpha+2} (1 - \eta_{\alpha+2}^{\alpha,\alpha+2}) \rangle}{2\kappa_2 \langle \eta_{\alpha+1}^{\alpha,\alpha+2} \rangle} \right] \quad (27)$$

$$a_-^{(2)} = \left[\frac{\langle (1 - \eta_{\alpha+1}^{\alpha,\alpha+2}) (1 - \eta_{\alpha+2}^{\alpha,\alpha+2}) \eta_{\alpha+3}^{\alpha,\alpha+2} \eta_{\alpha+4}^{\alpha,\alpha+2} \rangle}{\kappa_1 \langle \eta_{\alpha+3}^{\alpha,\alpha+2} \rangle} \right] + \left[\frac{\langle (1 - \eta_{\alpha+1}^{\alpha,\alpha+2}) (1 - \eta_{\alpha+2}^{\alpha,\alpha+2}) \eta_{\alpha+3}^{\alpha,\alpha+2} (1 - \eta_{\alpha+4}^{\alpha,\alpha+2}) \rangle}{2\kappa_2 \langle \eta_{\alpha+3}^{\alpha,\alpha+2} \rangle} \right] + \left[\frac{\langle \eta_{\alpha+1}^{\alpha,\alpha+2} (1 - \eta_{\alpha+2}^{\alpha,\alpha+2}) \eta_{\alpha+3}^{\alpha,\alpha+2} \eta_{\alpha+4}^{\alpha,\alpha+2} \rangle}{2\kappa_2 \langle \eta_{\alpha+3}^{\alpha,\alpha+2} \rangle} \right] + \left[\frac{\langle \eta_{\alpha+1}^{\alpha,\alpha+2} (1 - \eta_{\alpha+2}^{\alpha,\alpha+2}) \eta_{\alpha+3}^{\alpha,\alpha+2} (1 - \eta_{\alpha+4}^{\alpha,\alpha+2}) \rangle}{2\kappa_2 \langle \eta_{\alpha+3}^{\alpha,\alpha+2} \rangle} \right] \quad (28)$$

$$a_+^{(2)} = \left[\frac{\langle \eta_{\alpha+2}^{\alpha,\alpha+2} \eta_{\alpha+3}^{\alpha,\alpha+2} (1 - \eta_{\alpha+4}^{\alpha,\alpha+2}) \rangle}{\kappa_1 \langle \eta_{\alpha+3}^{\alpha,\alpha+2} \rangle} \right] + \left[\frac{\langle (1 - \eta_{\alpha+2}^{\alpha,\alpha+2}) \eta_{\alpha+3}^{\alpha,\alpha+2} (1 - \eta_{\alpha+4}^{\alpha,\alpha+2}) \rangle}{2\kappa_2 \langle \eta_{\alpha+3}^{\alpha,\alpha+2} \rangle} \right]. \quad (29)$$

Now, using the mean-field approximations where we write the three- and four-point correlations as a product of respective densities, we obtain the following coupled

set of four equations involving $a_{\pm}^{(1)}$, $a_{\pm}^{(2)}$, $\rho_{\pm}^{(1)}$ and $\rho_{\pm}^{(2)}$,

$$a_+^{(1)} = \frac{\rho_-^{(1)}(1 - \rho_-^{(2)})(1 - \rho_+^{(2)})}{\kappa_1} + \frac{(1 - \rho_-^{(1)})(1 - \rho_-^{(2)})(1 - \rho_+^{(2)})}{2\kappa_2} + \frac{\rho_-^{(1)}(1 - \rho_-^{(2)})\rho_+^{(2)}}{2\kappa_2} + \frac{(1 - \rho_-^{(1)})(1 - \rho_-^{(2)})\rho_+^{(2)}}{2\kappa_2} \quad (30)$$

$$a_-^{(1)} = \frac{(1 - \rho_-^{(1)})\rho_-^{(2)}}{\kappa_1} + \frac{(1 - \rho_-^{(1)})(1 - \rho_-^{(2)})}{2\kappa_2} \quad (31)$$

$$a_-^{(2)} = \frac{(1 - \rho_+^{(1)})(1 - \rho_-^{(2)})\rho}{\kappa_1} + \frac{(1 - \rho_+^{(1)})(1 - \rho_-^{(2)})(1 - \rho)}{2\kappa_2} + \frac{\rho_+^{(1)}(1 - \rho_-^{(2)})\rho}{2\kappa_2} + \frac{\rho_+^{(1)}(1 - \rho_-^{(2)})(1 - \rho)}{2\kappa_2} \quad (32)$$

$$a_+^{(2)} = \frac{\rho_-^{(2)}(1 - \rho)}{\kappa_1} + \frac{(1 - \rho_-^{(2)})(1 - \rho)}{2\kappa_2}. \quad (33)$$

To solve the set of coupled Eqs. 21 - 25 and Eqs. 30 - 33, we use *Mathematica* and obtain expressions for $\rho_{\pm}^{(1)}$ and $\rho_{\pm}^{(2)}$ as a function of global density ρ and v .

In Fig. 8, we plot $\rho_{\pm}^{(1)}$ and $\rho_{\pm}^{(2)}$ as a function of global density ρ (Fig. 8a) and defect velocity v (Fig. 8b and c) for various values of $q = 0, 0.2$ and 0.5 . For $q = 0$, the agreement between simulations and mean-field theory is excellent. For nonzero q , the agreement is good at the large velocity regime $v \gg q$. However, some discrepancies are observed for $v \lesssim q$. Also, note that the numerical values of $\rho_{\pm}^{(1)}$ and $\rho_{\pm}^{(2)}$ (or, $\rho_+^{(1)}$ and $\rho_-^{(2)}$) are close but they are not exactly equal. Moreover, as we show below, unlike the cases of the two defects with $R = 1$ discussed in the previous subsection, there is no particle-hole symmetry for two defects with $R = 2$, even within mean-field theory.

To calculate the current within mean-field theory, we note that, for $q \neq 0$, the following five bonds actually contribute to the current during the defect residence time τ . The individual diffusive currents, $J_{i,i+1}$ across the bond between the sites i and $i + 1$, are given below,

$$\begin{aligned} J_{\alpha-1,\alpha} &= \tilde{q}[\rho(1 - \rho_-^{(1)}) - \rho_-^{(1)}(1 - \rho)] = \tilde{q}(\rho - \rho_-^{(1)}), \\ J_{\alpha,\alpha+1} &= -\tilde{p}[\rho_+^{(1)}(1 - \rho_-^{(1)})], \\ J_{\alpha+1,\alpha+2} &= \tilde{p}[\rho_+^{(1)}(1 - \rho_-^{(2)})], \\ J_{\alpha+2,\alpha+3} &= -\tilde{p}[\rho_+^{(2)}(1 - \rho_-^{(2)})], \\ J_{\alpha+3,\alpha+4} &= \tilde{p}[\rho_+^{(2)}(1 - \rho)] \end{aligned}$$

where the effective Poisson rates are $\tilde{p} = (v/L)(1 - e^{-p/2v})$ and $\tilde{q} = (v/L)(1 - e^{-q/2v})$. The net current can

be obtained by adding all these individual contributions

$$J_q(\rho, v) = J_{\alpha-1,\alpha} + J_{\alpha,\alpha+1} + J_{\alpha+1,\alpha+2} + J_{\alpha+2,\alpha+3} + J_{\alpha+3,\alpha+4}. \quad (34)$$

which we compare with the simulations in Fig. 9. The agreement between simulations and mean-field theory is reasonably good for large $v \gg q$. For intermediate velocity $v \lesssim q$, mean-field theory breaks down due to non-trivial spatial correlations; however, it still captures the broad features like current reversal as a function of defect velocity or density.

Note that, if we assume $\rho_+^{(1)} \approx \rho_+^{(2)} = \rho_+$ (which is indeed the case as seen in Fig. 8), two currents $J_{\alpha+1,\alpha+2}$ and $J_{\alpha+2,\alpha+3}$ cancel each other. Further assuming $\rho_-^{(1)} \approx \rho_-^{(2)} = \rho_-$, we obtain, to a good approximation, the net current

$$J_q(\rho, v) \simeq \tilde{p}\rho_+(\rho_- - \rho) + \tilde{q}(\rho_- - \rho), \quad (35)$$

which matches the expression for net current derived in the case of a single moving defect in [40]. We verify this in Figs 10 and 11, where we plot the scaled current JL against ρ and v , respectively, and compare with our data in the single defect case. We find for large $v \geq q$, the current is indeed same in the two cases but for smaller $v \ll q$, there is a significant difference. The above analysis can be extended to arbitrary n number of defects located at alternate sites $\alpha_{k+1} = \alpha_k + 2$ with $k = 1, \dots, (n-1)$.

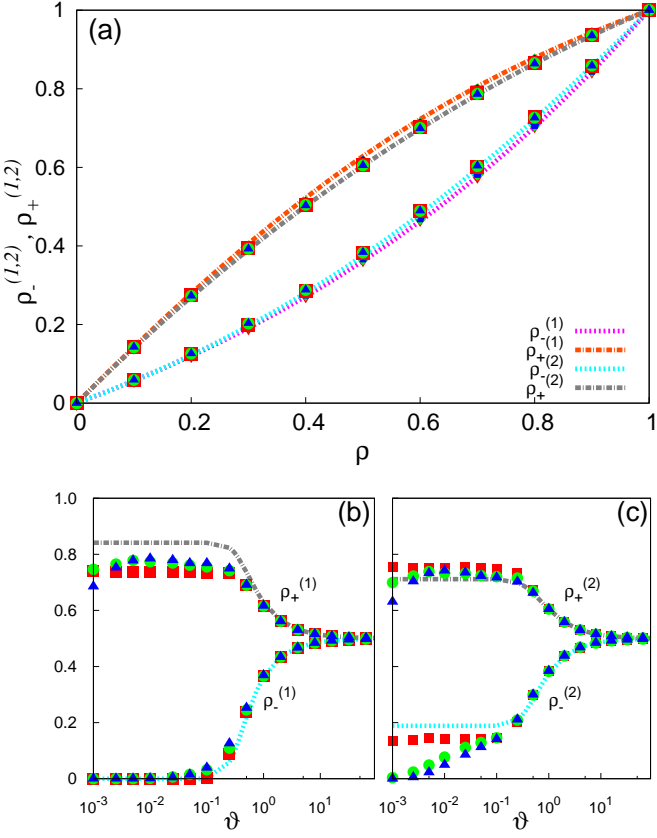


FIG. 8: (Color online) Two defects separated by distance $R = 2$. (a): Variation of $\rho_{\pm}^{(1)}$ and $\rho_{\pm}^{(2)}$ with global density ρ for various values of q with $v = 1.0$, $p = 1$, and $r = 0$. (b) and (c): Variation of $\rho_{\pm}^{(1)}$ and $\rho_{\pm}^{(2)}$ with defect velocity v for various q with $\rho = 0.5$, $p = 1$ and $r = 0$. Here, $q = 0$ (red squares), 0.2 (green circles) and 0.5 (blue triangles). Lines are obtained from mean-field theory and discrete points from simulations.

C. $R \geq 3$: Two defects separated by three or more lattice spacing

In this section, we consider the case when the defect sites are separated by three or more lattice spacing $R \geq 3$. We present explicit results for $R = 3$, and these results can be easily extended to the cases with $R > 3$. Let us assume the defect sites are located at α and $\alpha + 3$. Recall that the density pattern created by a single defect consists of a trough at the defect site and a bump at the next site. Therefore, when the two defects are at a distance $R = 3$, the density pattern created around each

of them do not overlap and as a result, the local density at site $\alpha + 2$ remains same as the bulk density. From this simple consideration, we formulate the ansatz,

$$\langle \rho_{st}^{1,4} | = \left\{ \rho_{-}^{(1)}, \rho_{+}^{(1)}, \rho_b, \rho_{-}^{(2)}, \rho_{+}^{(2)}, \rho_b, \dots, \rho_b \right\}, \quad (36)$$

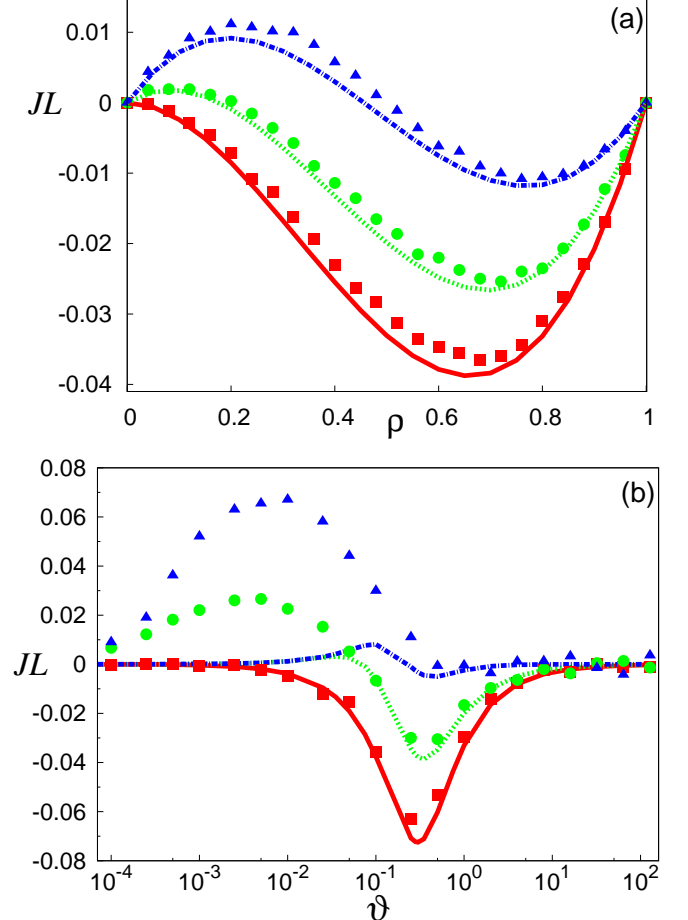


FIG. 9: (Color online) Two defects separated by distance $R = 2$. (a): Variation of the scaled current JL with global density ρ for $v = 1$. (b): Variation of the scaled current JL with defect velocity v for $\rho = 0.5$. Here, $q = 0$ (red squares), 0.2 (green circles) and 0.5 (blue triangles) and $p = 1$ and $r = 0$. Solid lines are from mean-field theory and points from simulations.

where, at the time of measurement, the defects are at sites 1 and 4, and are about to move on to sites 2 and 5. The corresponding transition matrix has the form

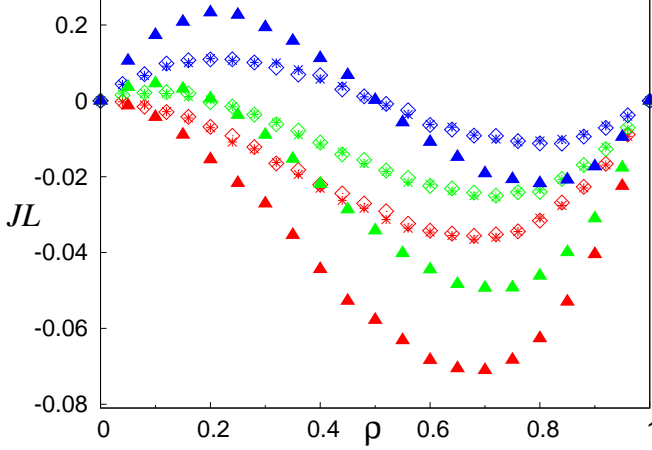


FIG. 10: (Color online) Comparison of scaled current JL vs. density ρ between three cases - (i) with a single defect (diamond; data from [40]) (ii) with two defects separated by distance $R = 2$ (asterix) and (iii) $R = 3$, where defects reside in next nearest neighbors (triangle), for various values of $q = 0$ (red), 0.2 (green), and 0.5 (blue); with $v = 1$, $p = 1$ and $r = 0$. Note that, for defect velocity $v \gtrsim q$ larger than bulk hopping rate, the two cases (i) and (ii) show approximately equal currents. For case (iii), the current is approximately doubled.

$$\mathcal{W}^{2,5} = \begin{bmatrix} 1 & 0 & 0 & 0 & 0 & 0 & 0 & \dots & 0 \\ a_-^{(1)} & \left(1 - a_+^{(1)} - a_-^{(1)}\right) & a_+^{(1)} & 0 & 0 & 0 & 0 & \dots & 0 \\ 0 & 0 & 1 & 0 & 0 & 0 & 0 & \dots & 0 \\ 0 & 0 & 0 & 1 & 0 & 0 & 0 & \dots & 0 \\ 0 & 0 & 0 & a_-^{(2)} & \left(1 - a_+^{(2)} - a_-^{(2)}\right) & a_+^{(2)} & 0 & \dots & 0 \\ 0 & 0 & 0 & 0 & 0 & 1 & 0 & \dots & 0 \\ \dots & \dots \\ 0 & 0 & 0 & 0 & 0 & 0 & \dots & 0 & 1 \end{bmatrix}$$

which acts on the above state vector $\langle \rho_{st}^{1,4} |$ to give the new state vector $\langle \rho_{st}^{2,5} | = \{ \rho_b, \rho_-^{(1)}, \rho_+^{(1)}, \rho_b, \rho_-^{(2)}, \rho_+^{(2)}, \rho_b, \dots, \rho_b \}$, i.e.,

$$\langle \rho_{st}^{2,5} | = \langle \rho_{st}^{1,4} | \mathcal{W}^{2,5}. \quad (37)$$

The steady-state condition Eq. 37 yields exactly the same relations, between density peaks, troughs and the conditional probabilities, as given in Eqs. 22 - 25. The conditional probabilities $a_{\pm}^{(1)}$ and $a_{\pm}^{(2)}$, within mean-field approximation, can be written as

$$a_+^{(1)} = \frac{(1 - \rho) \rho_-^{(1)}}{\kappa_1} + \frac{(1 - \rho)(1 - \rho_-^{(1)})}{2\kappa_2}, \quad (38)$$

$$a_-^{(1)} = \frac{(1 - \rho_-^{(1)})\rho}{\kappa_1} + \frac{(1 - \rho)(1 - \rho_-^{(1)})}{2\kappa_2}, \quad (39)$$

and

$$a_+^{(2)} = \frac{(1 - \rho) \rho_-^{(2)}}{\kappa_1} + \frac{(1 - \rho)(1 - \rho_-^{(2)})}{2\kappa_2}, \quad (40)$$

$$a_-^{(2)} = \frac{(1 - \rho_-^{(2)})\rho}{\kappa_1} + \frac{(1 - \rho)(1 - \rho_-^{(2)})}{2\kappa_2} \quad (41)$$

which are however different from Eqs. 30 - 33. Note that the two sets of equations - one involving $\rho_{\pm}^{(1)}$ and $a_{\pm}^{(1)}$ (Eqs 22, 23 and 39) and the other involving $\rho_{\pm}^{(2)}$ and $a_{\pm}^{(2)}$ (Eqs 24, 25 and 41)- are decoupled from each other and imply $\rho_{\pm}^{(1)} = \rho_{\pm}^{(2)} = \rho_{\pm}$. The above analysis can be straightforwardly extended to arbitrary number of defects, which are separated from each other by three or more lattice spacings. Therefore, on the mean-field

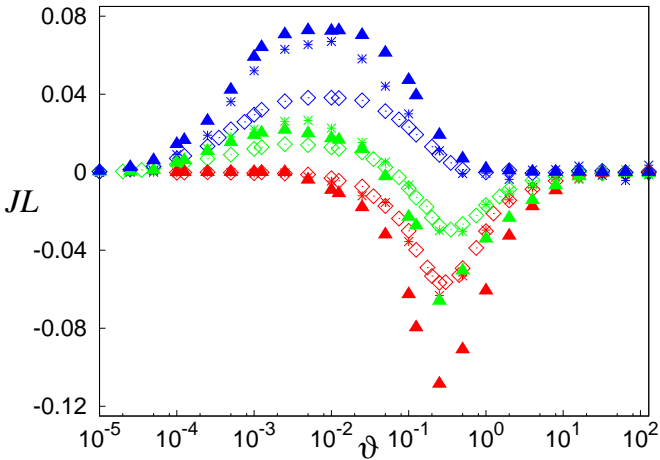


FIG. 11: (Color online) Comparison of scaled current JL vs. velocity v between three cases - (i) with a single defect (diamond), (ii) with two defects separated by distance $R = 2$ (asterix) and (iii) $R = 3$, where defects reside at next nearest neighbors (triangle), for various values of $q = 0$ (red), 0.2 (green), and 0.5 (blue); with $\rho = 0.5$, $p = 1$ and $r = 0$ are fixed throughout. At larger velocity $v \gg q$, the currents in cases (i) and (ii) are approximately same. On the other hand, at smaller velocity $v \lesssim q$, the currents in cases (ii) and (iii) are quite close.

level, two (or more) defects separated by distance $R \geq 3$ do not have any effect on each other and act as collection of two (or more) isolated defects. Consequently, the time-averaged current can be written as sum of the two contributions arising from each of the defects,

$$J_q(\rho, v) = 2[\tilde{p}\rho_+(\rho_- - \rho) + \tilde{q}(\rho_- - \rho)], \quad (42)$$

which may be compared with Eq. 35, the current in the case of $R = 2$.

IV. SSEP WITH ORDERED SEQUENTIAL UPDATE

In this section, we show that a close connection exists between our system of SSEP with a single moving defect and an SSEP with ordered (sitewise) sequential update. In the latter process, N hardcore (otherwise non-interacting) particles are considered on a ring consisting of L sites and, in each Monte Carlo step, the L sites of the lattice are updated sequentially in a particular order. For example, site 1 is chosen first and if there is a particle present on that site, it hops to any of the nearest neighbor sites with equal probability, provided the hardcore exclusion is satisfied. Then site 2 is chosen and the same process is repeated. After that site 3 is chosen and so on. This way all the sites on the lattice are accessed sequentially and updated. When the L -th update is performed on the L -th site, that concludes one Monte Carlo step.

Note that the sequential movement of the update-site is very similar to the movement of a single defect site in the limit $q = 0$, $r = 0$ and $v = L$. In other words, one could think of an infinite potential barrier present at the position of a single defect, which moves one lattice unit in every micro time-step and consequently performs one complete cycle every Monte Carlo step. Since no bulk hopping is allowed, in this case, hopping can take place only at the defect site, nowhere else on the lattice. This model of SSEP with a single defect is just like the case of the SSEP with sitewise ordered sequential update, where particles can only hop out of the site, which is being updated at a particular time-step. As we show below, because of this connection, the structure of the density profile and the behavior of current in SSEP with sitewise ordered sequential update is very similar to what we find in the moving defect problem. There is, however, one subtle difference between these two models. In the moving-defect problem, the update sites are still chosen randomly and, when the defect site does not get selected, the occupancy of the system does not change. This is clearly different from sitewise ordered sequential update. As shown later, due to this important difference, strong correlations are observed for sitewise ordered sequential update, whereas mean-field theory is known to work rather well for the moving-defect problem with $q = 0$ and large v .

Time evolution equation for density in the case of sitewise ordered sequential updates can be written as

$$\langle \rho^{(\alpha+1)}(t_{\text{micro}} + 1) \rangle = \langle \rho^{(\alpha)}(t_{\text{micro}}) \rangle \mathcal{W}^{(\alpha+1)} \quad (43)$$

where matrix $\mathcal{W}^{(\alpha)}$ is the time evolution operator, i th element of the row vector $\langle \rho^{(\alpha)}(t_{\text{micro}}) \rangle$ represents the density at site i , α denotes the site which is being updated at a particular micro-time t_{micro} . The density is measured at the end of the update process at t_{micro} . The time evolution matrix $\mathcal{W}^{(\alpha)}$ can be straightforwardly constructed as in the previous cases of the SSEP with moving defects. For example, for specific values of $\alpha = 1$ and 2, $\mathcal{W}^{(\alpha)}$ can be explicitly written as given below

$$\mathcal{W}^{(1)} = \begin{bmatrix} (1 - a_+ - a_-) & a_+ & 0 & \dots & 0 & a_- \\ 0 & 1 & 0 & 0 & \dots & 0 \\ \dots & \dots & \dots & \dots & \dots & \dots \\ \dots & \dots & \dots & \dots & \dots & \dots \\ 0 & \dots & 0 & 0 & 1 & 0 \\ 0 & 0 & \dots & 0 & 0 & 1 \end{bmatrix},$$

$$\mathcal{W}^{(2)} = \begin{bmatrix} 1 & 0 & 0 & \dots & 0 & 0 \\ a_- & (1 - a_+ - a_-) & a_+ & 0 & \dots & 0 \\ 0 & 0 & 1 & 0 & \dots & 0 \\ \dots & \dots & \dots & \dots & \dots & \dots \\ 0 & \dots & 0 & 0 & 1 & 0 \\ 0 & 0 & \dots & 0 & 0 & 1 \end{bmatrix},$$

where the conditional probabilities

$$a_+ = \frac{\text{Prob}[\eta_{\alpha+2}^{(\alpha)} = 0 | \eta_{\alpha+1}^{(\alpha)} = 1]}{2}, \quad (44)$$

$$a_- = \frac{\text{Prob}[\eta_\alpha^{(\alpha)} = 0 | \eta_{\alpha+1}^{(\alpha)} = 1]}{2}, \quad (45)$$

can be calculated in terms of nearest neighbours correlations. Time-periodic steady-state density profile satisfies the following condition

$$\langle \rho_{st}^{(\alpha+1)} \rangle = \langle \rho_{st}^{(\alpha)} \rangle | \mathcal{W}^{(\alpha+1)}. \quad (46)$$

Without any loss of generality, we now consider $\alpha = 1$ and proceed with an ansatz for $\langle \rho_{st}^{(1)} \rangle = \{\rho_-, \rho_+, \rho_b, \dots, \rho_b, \rho_b\}$. From the condition Eq. 46, we have $\langle \rho_{st}^{(2)} \rangle = \langle \rho_{st}^{(1)} \rangle | \mathcal{W}^{(2)}$, leading to

$$\rho_+ = \frac{1}{1 - a_+} \rho_b > \rho_b, \quad (47)$$

$$\rho_- = \frac{1 - a_+ - a_-}{1 - a_+} \rho_b < \rho_b, \quad (48)$$

$$\rho_b = \frac{(1 - a_+)L}{2 - a_+ - a_- + (1 - a_+)(L - 2)} \rho \simeq \rho, \quad (49)$$

in the limit of large $L \gg 1$. Clearly, the density profile has the same spatial structure having a density peak and trough, moving with a velocity L per unit MC time. Time averaged particle current can be written as

$$J = \frac{1}{2} \left[\langle \eta_{\alpha+1}^{(\alpha)} (1 - \eta_{\alpha+2}^{(\alpha)}) \rangle - \langle \eta_{\alpha+1}^{(\alpha)} (1 - \eta_\alpha^{(\alpha)}) \rangle \right]. \quad (50)$$

Resorting to mean-field approximations, we get the following simple expressions,

$$\rho_+ = \frac{2\rho}{1 + \rho}, \quad (51)$$

$$\rho_- = \rho^2 \quad (52)$$

$$J = -\frac{\rho^2(1 - \rho)}{1 + \rho} < 0. \quad (53)$$

Here, the current is always opposite to the direction in which the ordered sequential updates are done and is *not* particle-hole symmetric. In Figs. 12 and 13 we compare the mean field predictions with simulation results. We find that, due to the nontrivial spatial correlations, the mean-field approximation does not work well here.

Previously, in Ref. [41], a *bondwise* ordered sequential update was studied where one after another bond (instead of sites) was chosen and updated. This particular update process however, satisfies detailed balance and yields the same steady-state weights as in an ordinary SSEP with usual random sequential update, i.e., uniform measure in the configuration space. Thus, the SSEP with bondwise ordered sequential update has a uniform density profile and does not have any current in the steady state. The sitewise ordered sequential update, on the other hand, shows a time-periodic steady state and a nonzero current as shown above.

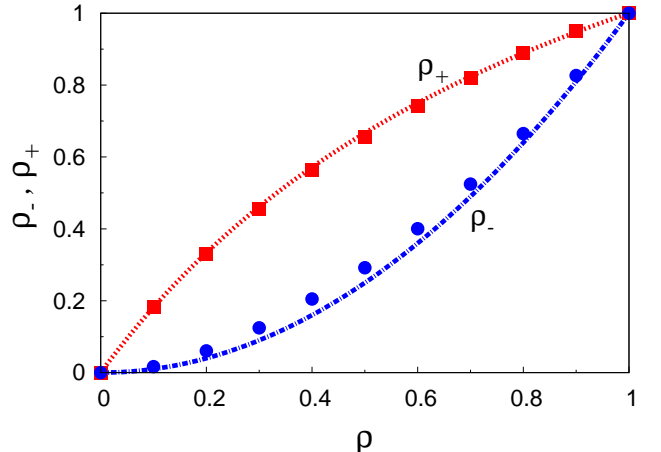


FIG. 12: (Color online) Density values ρ_+ and ρ_- at the peak and the trough are plotted as a function of ρ for ordered (sitewise) sequential update; system size $L = 128$. Solid lines and points are obtained from mean-field calculation and simulation, respectively.

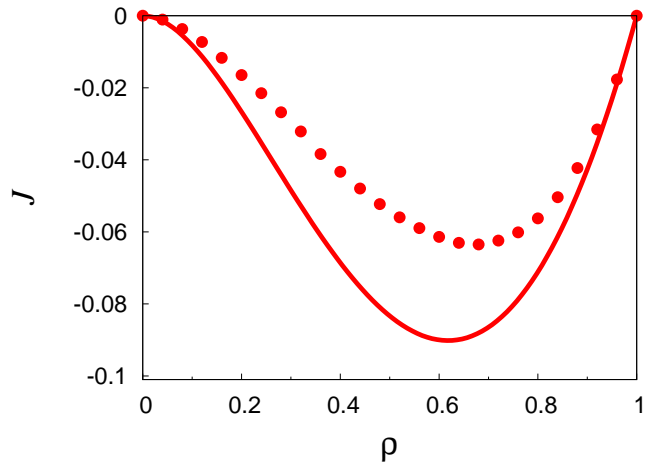


FIG. 13: (Color online) Current is plotted as a function of density ρ for ordered (sitewise) sequential update with system size $L = 128$. Solid line is obtained from the mean-field theory and points from numerical simulation. The reason for the discrepancy between mean-field theory and the simulation is due to the presence of nearest-neighbour correlations around the site where the update is done.

V. CONCLUSIONS

In this paper, we have studied the effect of time-periodic drive on a system of hardcore particles on a ring. We have modelled the effect of the drive by considering defects that move periodically on the lattice with uniform velocity. The particles diffuse on the lattice where the particle hopping rates, otherwise symmetric and uniform, are modified at and around the instantaneous position of the defects. Depending on these modified rates,

the defects act like a moving potential barrier or well. We have demonstrated that, in certain limits, this model can be mapped onto a simple symmetric exclusion process with sitewise ordered sequential updates.

Here, we have explored the collective effects of the moving defects on the spatial structure and transport in the system. When defects are far apart, they effectively act like a collection of single individual defects. However, when the defects are close, spatial structures may be quite complex, e.g., multiple peaks and troughs could develop in travelling density wave. Consequently, the particle current is described by fourth or higher order spatial correlations. In particular, when the defects occupy nearest neighbour positions on the lattice, in the limit of large defect velocity, the current shows particle-hole symmetry, which is not seen in any other cases. In general, the particle current shows polarity reversal and nonmonotonicity upon variation of particle density and defect velocity.

For simplicity, here we have considered an infinite potential barrier, i. e., $r = 0$, which strictly forbids any particle to hop into the defect sites. A finite barrier would mean $r \neq 0$. In that case, we have verified (data not shown here) that the qualitative behaviours of the density profile and the current do not change. A nonzero r merely tends to homogenize the density variations around the defect sites by reducing the height (depth) of the density peaks (troughs). Also, throughout the paper, we have considered defects which act like potential barrier,

i.e., $p > r$. One may ask what happens for $p < r$, i.e., when a potential well is present instead. However, since a particle hopping out of a defect site (or into the defect site) with rate p (rate r) can equivalently be described as a hole hopping into (or out of) the defect site with the same rate, the density profile and the current for the moving potential well can be obtained simply by substituting $\rho \rightarrow 1 - \rho$ (interchanging the particles and holes) and $J \rightarrow -J$ in the respective quantities in the case of the barrier.

In all the cases discussed in this paper, the striking features in particle transport such as polarity reversal and appearance of multiple peaks in particle current as a function of defect velocity and density, remarkably persist, irrespective of the microscopic details. In fact, we have verified (data not presented here) that these features survive even in the presence of nearest-neighbour interactions among the hardcore particles. This leaves open the possibility of finding these features even in more realistic systems.

VI. ACKNOWLEDGEMENTS

We thank S. S. Manna for very useful discussions. R.C. acknowledges the support from IMSc/DAE and DGAPA/UNAM postdoctoral fellowships.

[1] D. J. Thouless, Phys. Rev. B **27**, 6083 (1983).
[2] M. Switkes *et al.*, Science **283**, 1905 (1999); P. Leek *et al.*, Phys. Rev. Lett. **95**, 256802 (2005).
[3] S. Watson *et al.*, Phys. Rev. Lett. **91**, 258301 (2003).
[4] R. D. Astumian, Phys. Rev. Lett. **91**, 118102 (2003). R. D. Astumian and P. Hanggi, Phys. Today **55**, 33 (2002).
[5] S. Rahav, J. Horowitz, and C. Jarzynski, Phys. Rev. Lett. **101**, 140602 (2008).
[6] R. Marathe, A. M. Jayannavar, and A. Dhar, Phys. Rev. E **75**, 030103 (2007).
[7] F. Julicher, A. Ajdari, and J. Prost, Rev. Mod. Phys. **69**, 1269 (1997); P. Reimann, Phys. Rep. **361**, 57 (2002).
[8] F. Marchesoni, Phys. Rev. Lett. **77**, 2364 (1996).
[9] U. Seifert, Phys. Rev. Lett. **106**, 020601 (2011).
[10] K. Jain, R. Marathe, A. Chaudhuri, and A. Dhar, Phys. Rev. Lett. **99**, 190601 (2007).
[11] R. Marathe, K. Jain, and A. Dhar, J. Stat. Mech. P11014 (2008).
[12] D. Chaudhuri and A. Dhar, EPL **94**, 30006 (2011).
[13] D. Chaudhuri, A. Raju, and A. Dhar, Phys. Rev. E **91**, 050103 (2015).
[14] A. Simon and A. Libchaber, Phys. Rev. Lett. **68**, 3375 (1992); L. P. Faucheux, G. Stolovitzky, and A. Libchaber, Phys. Rev. E **51**, 5239 (1995).
[15] T. M. Squires and S. R. Quake, Rev. Mod. Phys. **77**, 977 (2005).
[16] R. F. Service, Science **282**, 399 (1998).
[17] H. Gau, S. Herminghaus, P. Lenz, and R. Lipowsky, Science **283**, 46 (1999).
[18] A. Terray, J. Oakey, and D. W. M. Marr, Science **296**, 1841 (2002).
[19] F. Penna and P. Tarazona, J. Chem. Phys. **119**, 1766 (2003).
[20] P. Tarazona and U. M. B. Marconi, J. Chem. Phys. **128**, 164704 (2008).
[21] R. van Zon and E. G. D. Cohen, Phys. Rev. E **67**, 046102 (2003).
[22] R. van Zon and E. G. D. Cohen, Phys. Rev. Lett. **91**, 110601 (2003).
[23] A. Pal and S. Sabhapandit, Phys. Rev. E **87**, 022138 (2013).
[24] G. M. Wang, E. M. Sevick, E. Mittag, D. J. Searles, and D. J. Evans, Phys. Rev. Lett. **89**, 050601 (2002).
[25] V. Bickle, T. Speck, L. Helden, U. Seifert, and C. Bechinger, Phys. Rev. Lett. **96**, 070603 (2006). V. Bickle, T. Speck, C. Lutz, U. Seifert, and C. Bechinger, Phys. Rev. Lett. **98**, 210601 (2007).
[26] T. Bohlein and C. Bechinger, Phys. Rev. Lett. **109**, 058301 (2012).
[27] J. R. Gomez-Solano, A. Petrosyan, S. Ciliberto, R. Chetrite, and K. Gawedzki, Phys. Rev. Lett. **103**, 040601 (2009). J. R. Gomez-Solano, L. Bellon, A. Petrosyan, and S. Ciliberto, EPL **89**, 60003 (2010).
[28] F. Spitzer, Adv. Math. **5**, 246 (1970).
[29] T. M. Liggett, *Interacting Particle Systems*, Springer, New York (1985). G. M. Schtz, in *Phase Transitions and*

Critical Phenomena, edited by C. Domb and J. Lebowitz (Academic, New York, 2000), pp. 3 - 242.

[30] H. Spohn, J. Phys. A **16** 4275 (1983).

[31] G. Schutz and S. Sandoval, Phys. Rev. E **49**, 2726 (1994).

[32] J. E. Santos and G. M. Schutz, Phys. Rev. E **64**, 036107 (2001).

[33] B. Derrida, J. L. Lebowitz, and E. R. Speer, Phys. Rev. Lett. **87**, 150601 (2001); T. Bodineau and B. Derrida, Phys. Rev. Lett. **92**, 180601 (2004).

[34] J. Karger and D.M. Ruthven, *Diffusion in Zeolites and Other Microporous Solids*, Wiley New York 1992. A. Brzank, Diffusion Fundamentals **4**, 7.1 - 7.12 (2006).

[35] A. Nagar, M. Ha, and H. Park, Phys. Rev. E **77**, 061118 (2008).

[36] C. Appert-Rolland, B. Derrida, V. Lecomte, and F. van Wijland, Phys. Rev. E **78**, 021122 (2008).

[37] T. Sadhu, S. N. Majumdar, and D. Mukamel, Phys. Rev. E **84**, 051136 (2011).

[38] C. Hegde, S. Sabhapandit, and A. Dhar, Phys. Rev. Lett. **113**, 120601 (2014).

[39] C. Arita, P. L. Krapivsky, and K. Mallick, Phys. Rev. E **90**, 052108 (2014).

[40] R. Chatterjee, S. Chatterjee, P. Pradhan, and S. S. Manna, Phys. Rev. E **89**, 022138 (2014).

[41] N. Rajewsky, L. Santen, A. Schadschneider, and M. Schreckenberg, J. Stat. Phys. **92**, 151 (1998).